Inorg. Chem. **2004**, *43*, 874–881

Inorganic Chemistry
Article

New Insights into the Structural and Dynamical Features of Lithium Hexaoxometalates Li_7MO_6 (M = Nb, Ta, Sb, Bi)

Claus Mühle, Robert E. Dinnebier, Leo van Wüllen, Georg Schwering, and Martin Jansen*

Max-Planck-Institute for Solid State Research, Heisenbergstrasse 1, D-70569 Stuttgart, Germany

Received June 23, 2003

We present a (re)investigation of the hexaoxometalates Li_8MO_6 (M = Sn, Pb, Zr, Hf) and Li_7MO_6 (M = Nb, Ta, Sb, Bi). Lithium motion and ionic conductivity in the hexaoxometalates were studied using impedance spectroscopy (for Li_7MO_6, M = Sb, Bi, Ta) and ^6Li and ^7Li solid-state nuclear magnetic resonance (for Li_7TaO_6). The NMR data indicate a considerable exchange of Li among the tetrahedral and octahedral voids even at ambient temperature. In an investigation of the crystal structures using laboratory and synchrotron X-ray powder diffraction techniques, the structures of Li_7TaO_6, Li_7NbO_6, and Li_7SbO_6 could be solved and refined. All three reveal a triclinic metric (Li_7SbO_6, triclinic, $P\bar{1}$, $a = 5.38503(6)$ Å, $b = 5.89164(7)$ Å, $c = 5.43074(6)$ Å, $\alpha = 117.2210(6)°$, $\beta = 119.6311(6)°$, $\gamma = 63.2520(7)°$, $V = 127.454(3)$ Å^3, $Z = 1$; Li_7NbO_6, triclinic, $P\bar{1}$, $a = 5.37932(9)$ Å, $b = 5.91942(11)$ Å, $c = 5.37922(9)$ Å, $\alpha = 117.0033(9)°$, $\beta = 119.6023(7)°$, $\gamma = 63.2570(9)°$, $V = 126.938(4)$ Å^3, $Z = 1$; Li_7TaO_6, triclinic, $P\bar{1}$, $a = 5.38486(2)$ Å, $b = 5.92014(3)$ Å, $c = 5.38551(2)$ Å, $\alpha = 117.0108(2)°$, $\beta = 119.6132(2)°$, $\gamma = 63.2492(2)°$, $V = 127.208(1)$ Å^3, $Z = 1$.

Introduction

Alkali-metal salts of the hexaoxometalates have been known since their first mention by Scholder in 1958, who described compounds of the type Li_8MO_6 (M = Sn,[1−5] Pb,[1,3,6] Zr,[1,3] Hf[4]). The most prominent characteristic of the powder diffraction patterns of Li_7MO_6 (M = Nb,[1,7] Ta,[1,7−9] Sb,[1,10] Bi[7]) and Li_8MO_6 is their close resemblence, indicating that these compounds are isostructural. The common structural motif for the hexaoxometalates is a hexagonal close packing of oxygen atoms with lithium atoms occupying tetrahedral and octahedral voids; thus, in Li_7MO_6 some of the lithium atom positions are not fully occupied.[11] It is the generation of vacancies within the parent Li_8MO_6 structure that renders the members of the Li_7MO_6 family promising candidates for lithium ion conducting materials.

The first structure determination based on single-crystal structure data was published for Li_8TbO_6,[1] followed by Li_8SnO_6[4,5] and Li_8PbO_6,[6] all of which crystallize in $R\bar{3}$. Hoppe and Wehrum[8] determined the structure of Li_7TaO_6 using single-crystal data ($P3$, $a = 5.358$ Å, $c = 15.073$ Å, $Z = 3$), thus confirming the close structural relationship to Li_8SnO_6.

Some of the lithium hexaoxometalates have already been investigated by IR and Raman spectroscopy. In 1974, Müller, Baran, and Hauck[12] pointed out that it is not possible to exactly correlate the valence vibrations to the MO_6 octahedra in the IR spectra due to a very strong absorption. They observed a strong band in all Raman spectra and assigned it to the symmetric valence vibration of the octahedra. They also calculated the force constants for the ν_s(MO) vibration.

The ionic conductivities of Li_8MO_6 (M = Sn, Zr) and Li_7MO_6 (M = Nb, Ta) were first measured by Delmas et al.[13] in 1979, followed by Brice and Ramdani[14] in 1981 with Li_8MO_6 (M = Ce, Hf). According to their results, these substances show high ionic conductivities. Li_7BiO_6 proved to be the best lithium ion conductor among the lithiumhexaoxometalates.[15,16]

---

* Author to whom correspondence should be addressed. E-mail: m.jansen@fkf.mpg.de. Fax: (+49) 711-689-1502.

(1) Scholder, R.; Gläser, H. *Z. Anorg. Allg. Chem.* **1964**, *327*, 15.
(2) Scholder, R. *Angew. Chem.* **1958**, *70*, 583.
(3) Räde, D. Ph.D. Thesis, University of Karlsruhe, Germany, 1958.
(4) Trömel, M.; Hauck, J. *Z. Anorg. Allg. Chem.* **1969**, *368*, 248.
(5) Hoppe, R.; Braun, R. M. *Z. Anorg. Allg. Chem.* **1977**, *433*, 181.
(6) Brazel, B.; Hoppe, R. *Z. Anorg. Allg. Chem.* **1984**, *515*, 81−86.
(7) Braun, R. M. Diploma Thesis, University of Giessen, Germany, 1976.
(8) Wehrum, G.; Hoppe, R. *Z. Anorg. Allg. Chem.* **1994**, *620*, 659.
(9) Hauck, J. *Z. Naturforsch., Sect. B* **1969**, *24*, 1067.
(10) Hauck, J. *Z. Naturforsch., Sect. B* **1969**, *24*, 252.
(11) Hauck, J. *Z. Naturforsch., Sect. B* **1969**, *24*, 1347.
(12) Müller, A.; Baran, E. J.; Hauck, J. *Spectrochim. Acta, Sect. A* **1975**, *31*, 801−803.
(13) Delmas, C.; Maazaz, A.; Guillen, F. *Mater. Res. Bull.* **1979**, *14*, 619−625.
(14) Brice, J.-F.; Ramdani, A. *Mater. Res. Bull.* **1981**, *16*, 1487−1492.

10.1021/ic030208w CCC: $27.50

In this work, we present a reinvestigation of the crystal structures of the hexaoxometalates. The previously unknown structures of Li_7MO_6 (M = Nb, Ta, Sb) are solved and refined from high-resolution X-ray powder diffraction data. In addition, the lithium conductivity in Li_7MO_6 was studied using impedance spectroscopy and correlated to the phase transitions found in differential scanning calorimetry (DSC) measurements. The nature of the Li mobility—studied exemplarily on Li_7TaO_6—was traced using solid-state nuclear magnetic resonance spectroscopy.

Experimental Section

Syntheses. The lithium hexaoxometalates have been synthesized by solid-state reaction of mixtures of the respective metal oxides with a stoichiometric amount of lithium oxide under dry argon or of lithium hydroxide in a stream of dry oxygen (5% surplus was required for pure products). Li_2O has been prepared as described[17] by dehydrating $LiOH{\cdot}H_2O$ (Fluka, 99+%) in a vacuum at $T = 800$ °C. All products are colorless and air-sensitive powders.

Li_7TaO_6. Ta_2O_5 (Fluka, 99.9%) was blended with Li_2O and heated at $T = 700$ °C for 2 days in a silver crucible sealed in a quartz ampule under a dry argon atmosphere.

Li_7NbO_6. Nb_2O_5 (Merck, 99+%) was heated with a 7% surplus of lithium oxide at $T = 900$ °C for 2 days in a sealed tantalum crucible under dry argon.

Li_7SbO_6/Li_7BiO_6/Li_8SnO_6/Li_8PbO_6. Mixtures of Sb_2O_3 (Sigma-Aldrich, 99.99%)/Bi_2O_3 (Merck, 99.9%)/SnO_2 (Alfa-Aesar, 99.99%)/PbO_2 (Alfa-Aesar, 99.99%) and $LiOH{\cdot}H_2O$ were heated in nickel boats in a stream of dry oxygen at $T = 700$ °C for 1 day.

Li_8ZrO_6/Li_8HfO_6. ZrO_2 (Alfa-Aesar, 99+%)/HfO_2 (Chempur, 99.95%) and Li_2O were mixed and heated at $T = 600$ °C for 2 days in a silver crucible sealed in a quartz ampule under dry argon.

Characterization. High-resolution X-ray powder diffraction data of Li_7TaO_6 were collected at $T = 295$ K on beamline X3B1 of the Brookhaven National Synchrotron Light Source in transmission geometry with the samples sealed in a lithium borate glass capillary of 0.3 mm diameter (Hilgenberg glass no. 50). X-rays of wavelength 0.65 Å were selected by a double Si(111) monochromator. Wavelengths and the zero point were determined from eight well-defined reflections of the NBS1976 flat plate alumina standard. The diffracted beam was analyzed with a Ge(111) crystal and detected with a Na(Tl)I scintillation counter employing a pulse height discriminator in the counting chain. The incoming beam was monitored by an ion chamber for normalization purposes to take the decay of the primary beam into account. In this parallel beam configuration, the resolution is determined by the analyzer crystal instead of slits.[18] Data were taken in steps of 0.004° from $2\theta = 6°$ to $2\theta = 22.0°$ for 2.1 s and from $2\theta = 22°$ to $2\theta = 50.13°$ for 7.1 s (see Table 1). Although θ scans did not show serious crystallite size effects, the samples were spun during measurement for better particle statistics. The powder pattern of Li_7TaO_6 exhibits several peaks of very small amounts (<0.5%) of $Li_{10}Ta_2O_{10}$ as an impurity phase. See Figure 1c for scattered X-ray intensities of Li_7TaO_6.

Table 1. Crystallographic Data of Li_7MO_7 (M = Nb, Sb, Ta)

	Li_7NbO_6	Li_7SbO_6	Li_7TaO_6
fw	237.47	266.32	332.45
space group	$P\bar{1}$ **(No. 2)**	$P\bar{1}$ **(No. 2)**	$P\bar{1}$ **(No. 2)**
a/Å	5.37932(9)	5.38503(6)	5.38486(2)
b/Å	5.91942(11)	5.89164(7)	5.92014(3)
c/Å	5.37922(9)	5.43074(6)	5.38551(2)
α/deg	117.0033(9)	117.2210(6)	117.0108(2)
β/deg	119.6023(7)	119.6311(6)	119.6132(2)
γ/deg	63.2570(9)	63.2520(7)	63.2492(2)
V/Å^3	126.938(4)	127.4537(30)	127.208(1)
Z	1	1	1
T/K	295	295	295
D_{calcd}/g cm^{-3}	3.107	3.469	4.340
radiation source, λ/Å	Cu Kα_1, 1.54059	Cu Kα_1, 1.54059	0.64992(2)
μ/cm^{-1}	183.18	414.97	167.11
$R_p{}^a$/%	8.0	5.3	7.8
$R_{wp}{}^a$/%	10.3	7.0	9.1
$R_{F^2}{}^a$/%	21.0	6.7	8.0

[a] R_p, R_{wp}, and R_{F^2} as defined in GSAS.[25]

X-ray powder diffraction data of Li_8MO_6 (M = Sn, Pb, Zr, Hf) and Li_7MO_6 (M = Nb, Sb, Bi) were collected at room temperature with a Stoe Stadi-P transmission laboratory diffractometer (primary beam Johansson-type Ge monochromator for Cu Kα_1 radiation, linear PSD) in steps of 0.01° over different ranges of 2θ for approximately 24 h each with the samples sealed in glass capillaries of 0.2 mm diameter (Hilgenberg glass no. 50). Further experimental details are given in Table 1. Different amounts of additional phases not exceeding 10% are present in the powder patterns. See Figure 1a,b for scattered X-ray intensities of Li_7SbO_6 and Li_7NbO_6.

Data reduction on all data sets was performed using the program WinXPow (Stoe) or GUFI.[19] Indexing with ITO[20] and TREOR[21] led to rhombohedral unit cells (space group $R\bar{3}$) for Li_8MO_6 (M = Sn, Pb, Zr, Hf) and Li_7BiO_6,[7] confirming the literature data. In the case of Li_7SbO_6,[1,10] Li_7NbO_6,[1,7] and Li_7TaO_6,[1,7,8] additional splittings of the reflections were observed, leading to triclinic unit cells. The lattice parameters of Li_7MO_6 (M = Nb, Ta, Sb) are given in Table 1. The number of formula units per unit cell could be determined to be $Z = 1$ from packing considerations and density measurements. $P\bar{1}$ was chosen as the most probable space group, which could later be confirmed by Rietveld refinements.[22] The peak profiles and precise lattice parameters were determined by LeBail-type fits[23] using the programs GSAS[24] and FULLPROF.[25] The background was modeled manually using GUFI. The peak profile was described by a pseudo-Voigt function in combination with a special function that accounts for the asymmetry due to axial divergence.[26,27]

From visual inspection, it was concluded that Li_7MO_6 (M = Nb, Ta, Sb) are isostructural and have a close relation to their Li_8MO_6 counterparts. Despite the similarity, it was not possible to refine the triclinic crystal structures with starting coordinates taken from

---

(15) Nomura, E.; Greenblatt, M. *J. Solid State Chem.* **1984**, *52*, 91−93.

(16) Nomura, E.; Greenblatt, M. *Solid State Ionics* **1984**, *13*, 249−254.

(17) Brauer, G. *Handbuch der Präparative Anorganische Chemie*; Ferdinand Enke Verlag: Stuttgart, Germany, 1978; Vol. 2, p 950.

(18) Cox, D. E. In *Handbook on Synchrotron Radiation*; Brown, G., Moncton, D. E., Eds.; Elsevier Science Publishers B.V.: Amsterdam, 1991; Vol. 3, p 155.

(19) Dinnebier, R. E. GUFI, Program for Measurement and Evaluation of Powder Pattern, Heidelberger Geowiss. Abh. 68, Heidelberg, Germany, 1993; ISBN 3-89257-067-1.

(20) Visser, J. W. *J. Appl. Crystallogr.* **1969**, *2*, 89−95.

(21) Werner, P.-E.; Eriksson, L.; Westdahl, L. *J. Appl. Crystallogr.* **1985**, *18*, 367−370.

(22) (a) Rietveld, H. M. *Acta Crystallogr.* **1967**, *22*, 151. (b) Rietveld, H. M. *J. Appl. Crystallogr.* **1969**, *2*, 65.

(23) LeBail, A.; Duroy, H.; Fourquet, J. L. *Mater. Res. Bull.* **1988**, *23*, 447−452.

(24) Larson, A. C.; von Dreele, R. B. *GSAS—General Structure Analysis System*; Los Alamos National Laboratory Report LAUR 86-748; Los Alamos National Laboratory: Los Alamos, NM, 1994; available by anonymous FTP from http://www.mist.lansce.lanl.gov.

(25) Rodríguez-Carvajal, J. Recent developments of the program FULLPROF. *Commission on Powder Diffraction Newsletter* 2001; Vol. 26, pp 12−19.

(26) Thompson, P.; Cox, D. E.; Hastings, J. B. *J. Appl. Crystallogr.* **1987**, *20*, 79−83.

(27) Finger, L. W.; Cox, D. E.; Jephcoat, A. P. *J. Appl. Crystallogr.* **1994**, *27*, 892−900.

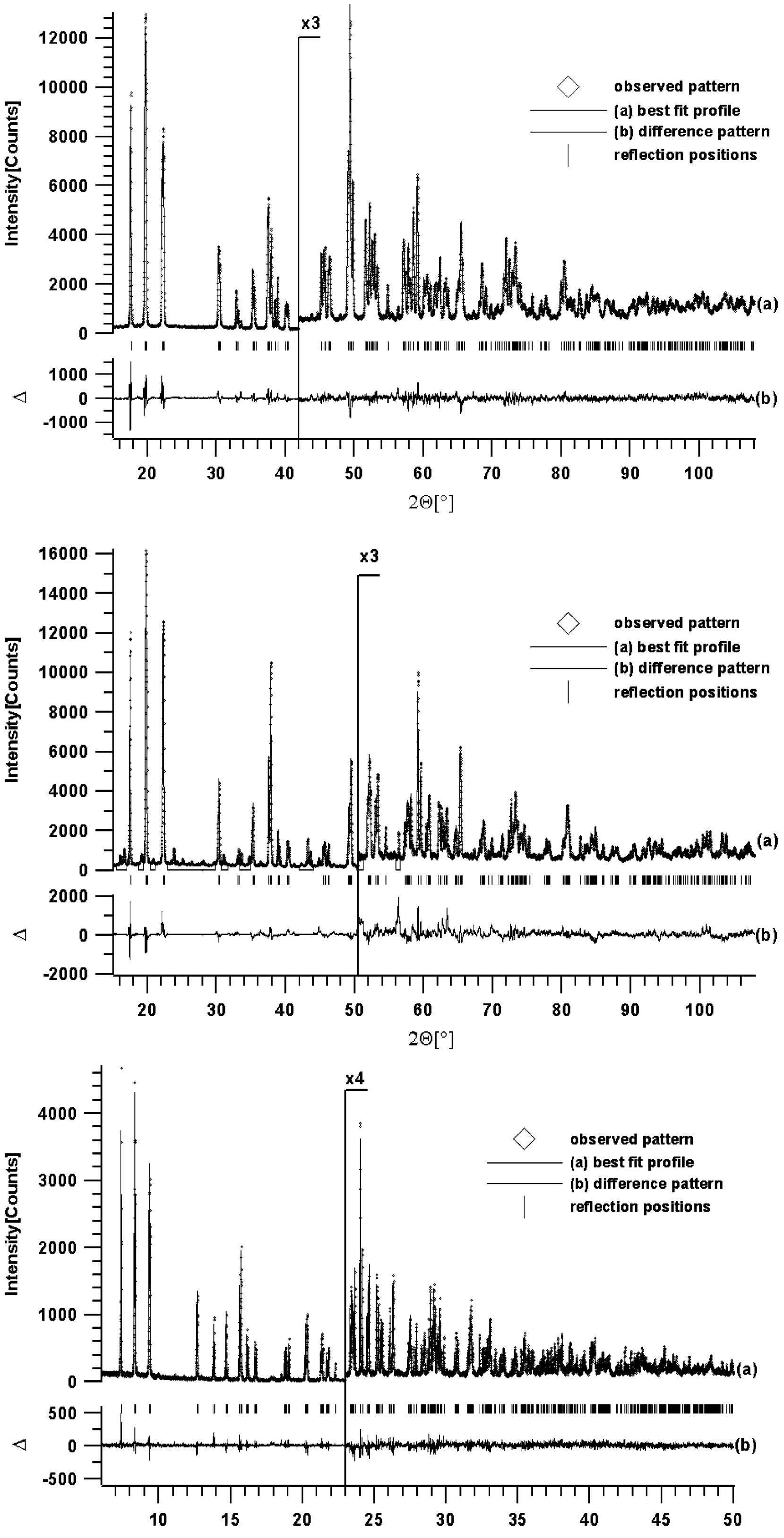

Figure 1. Scattered X-ray intensities for Li_7SbO_6 (a, top), Li_7NbO_6 (b, middle), and Li_7TaO_6 (c, bottom) at ambient conditions as a function of diffraction angle 2θ. Shown are the observed patterns (tilted squares), the best Rietveld fit profiles (line marked "a"), and the enlarged difference curves between observed and calculated profiles (line marked "b"). The high-angle parts are enlarged for clarity. The wavelengths were $\lambda = 1.54059$ Å for Li_7SbO_6 and Li_7NbO_6 and 0.65 Å for Li_7TaO_6. In the case of Li_7NbO_6 several excluded regions in the powder pattern have been defined, to account for small amounts of Li_2O and $Li_{10}Nb_2O_{10}$ present in the sample.

the rhombohedral unit cells. Therefore, the crystal structures of Li_7MO_6 (M = Nb, Ta, Sb) were solved ab initio by successive Rietveld refinements in combination with difference Fourier analysis using the program package GSAS (Figure 2). Due to the

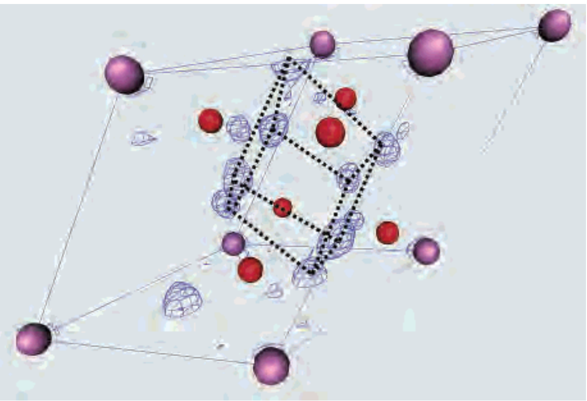

Figure 2. Perspective view of the crystal structure of Li$_7$TaO$_6$ showing the tantalum and the oxygen atoms. The positions of the lithium atoms (connected by dashed lines) are visualized by the isosurface of the three-dimensional difference electron density as obtained from Fourier analysis from a Rietveld refinement using only tantalum and oxygen atoms.

Table 2. Positional Parameters and Isotropic Temperature Factors for Li$_7$MO$_6$ (M = Sb, Nb, Ta)

atom	occupancy	x	y	z	*U*(eq)
Nb	1	0	0	0	1.53(2)
Sb		0	0	0	1.80(2)
Ta		0	0	0	1.52(2)
O1	1	0.9136(14)	0.2333(12)	0.3716(14)	2.61(9)
		0.9084(9)	0.2301(7)	0.3715(9)	2.47(6)
		0.9119(12)	0.2309(12)	0.3710(13)	2.16(2)
O2	1	0.2294(14)	0.2214(12)	0.0824(16)	2.61(9)
		0.2204(8)	0.2365(7)	0.0885(10)	2.47(6)
		0.2302(12)	0.2313(12)	0.0835(13)	1.87(14)
O3	1	0.3726(13)	0.7668(11)	0.2291(16)	2.61(9)
		0.3776(8)	0.7657(8)	0.2292(9)	2.47(6)
		0.3725(13)	0.7726(12)	0.2296(14)	2.46(16)
Lil	0.875	0.4880(50)	0.3534(47)	0.1210(60)	4.19(25)
		0.4943(30)	0.3870(28)	0.1215(34)	4.66(20)
		0.5026(33)	0.3657(31)	0.0855(36)	2.5
Li2	0.875	0.1040(40)	0.6475(47)	0.2500(50)	4.19(25)
		0.0992(32)	0.6261(29)	0.2426(35)	4.66(20)
		0.1116(32)	0.6616(32)	0.2648(33)	2.5
Li3	0.875	0.7640(50)	0.6347(47)	0.4920(50)	4.19(25)
		0.7709(29)	0.6427(31)	0.5107(39)	4.66(20)
		0.7590(32)	0.6281(31)	0.4899(34)	2.5
Li4	0.875	0.6410(50)	1.0404(27)	0.3240(50)	4.19(25)
		0.6535(35)	1.0325(21)	0.3482(30)	4.66(20)
		0.6569(37)	1.0079(24)	0.3255(38)	2.5

excellent reflection-to-parameter ratio, no soft constraints were necessary to stabilize the refinements. In all three cases, several Fourier cycles starting with the sole heavy atom located at the origin were necessary to achieve convergence. Agreement factors (*R* values) are given in Table 1, and the atomic coordinates in Table 2. A selection of intra- and intermolecular distances and angles is given in Table 3.

For the IR experiments, 1−2 mg of the samples and 500 mg of CsI were ground and pressed into pellets with 10 mm diameter. The spectra were measured in a vacuum using the Fourier transform spectrometer IFS 113v (Bruker, Germany).

The Raman spectra were obtained by measuring the samples sealed in a 1 mm quarz capillary under argon with a Raman spectrometer (Jobin Yvon, Japan).

Temperature-dependent Guinier recordings were conducted using the Guinier−Simon technique (Enraf-Nonius FR 553, CuKα_1, Johansson monochromator) in a temperature range from room temperature to $T = 500$ °C.

DSC data were recorded (model 404, Netzsch, Germany) by heating and cooling the sample in an aluminum crucible with a rate of 10 K/min from room temperature to $T = 500$ °C.

Table 3. Distances (Å) and Angles (deg) for Li$_7$MO$_6$ (M = Ta, Nb, Sb)[a]

	Li$_7$TaO$_6$	Li$_7$NbO$_6$	Li$_7$SbO$_6$
Ta−O(2)	1.989(6) × 2	1.956(9) × 2	1.973(5) × 2
Ta−O(1)	1.999(5) × 2	1.988(7) × 2	2.008(5) × 2
Ta−(O3)	2.008(9) × 2	2.014(6) × 2	2.033(4) × 2
O−Ta−O	89.5(3)−90.2(3)	89.2(3)−90.8(3)	88.9(2)−91.1(2)
	180.0(3)	180.0(3)	180.0(2)
Li(1)−O(2)	1.836(22)	1.770(37)	1.940(22)
Li(1)−O(1)	1.952(26)	1.980(21)	1.992(13)
Li(1)−O(3)	2.010(14)	2.077(37)	1.903(15)
Li(1)−O(3′)	2.053(17)	2.100(26)	2.021(20)
O−Li(1)−O	93.6(8)−121(1)	88(1)−121(2)	90.2(8)−116.2(9)
Li(2)−O(1)	1.819(20)	1.864(28)	1.882(19)
Li(2)−O(3)	1.910(26)	1.936(35)	2.050(24)
Li(2)−O(2)	1.981(15)	1.963(23)	1.957(15)
Li(2)−O(2′)	2.178(17)	2.153(26)	1.967(16)
O−Li(2)−O	93.2(9)−123(1)	92(1)−122(1)	88.6(6)−123(1)
Li(3)−O(1)	1.906(14)	1.897(32)	1.894(20)
Li(3)−O(3)	1.962(22)	1.904(20)	1.944(13)
Li(3)−O(1′)	2.007(17)	2.027(24)	2.069(16)
Li(3)−O(2)	2.037(19)	2.036(28)	1.939(22)
O−Li(3)−O	89.8(8)−120(1)	90(1)−123(2)	93.9(9)−122.1(7)
Li(4)−O(2)	2.144(14)	2.006(19)	2.156(13)
Li(4)−O(1)	2.167(25)	2.095(31)	2.095(22)
Li(4)−O(3)	2.195(20)	2.167(27)	2.101(16)
Li(4)−O(2′)	2.223(21)	2.264(27)	2.405(17)
Li(4)−O(3)	2.245(24)	2.365(29)	2.306(20)
Li(4)−O(1′)	2.336(15)	2.467(19)	2.365(13)
O−Li(4)−O	77.3(5)−96.5(7)	75.6(6)−104(1)	77.6(4)−99.8(8)
	170.3(9)−174(1)	166(1)−172(1)	168.5(7)−171.5(8)
Li(4)−Li(2)	2.410(20)	2.424(28)	2.481(19)
Li(4)−Li(1)	2.586(30)	2.209(42)	2.512(26)
Li(4)−Li(3)	2.561(23)	2.461(34)	2.434(22)
Li(2)−Li(3)	2.290(31)	2.299(47)	2.193(32)
Li(2)−Li(1)	2.364(23)	2.205(32)	2.187(24)
Li(1)−Li(3)	2.225(20)	2.289(33)	2.225(20)
Li−Li−Li	74.6(8)−101.6(8)	79(1)−105(1)	75.5(7)−99.2(8)

[a] The esd values from Rietveld refinement are given in parentheses.

The electric conductivity was determined with ion-blocking silver electrodes using compact polycrystalline powder samples (diameter 6 mm, thickness 0.5−1 mm, pressed with $p = 350$ MPa). The samples were located in a glass cell[28] under dry argon. Temperature-dependent impedance spectroscopy and the ac conductivity were measured with a computer-controlled impedance bridge (4192A LF, Hewlett-Packard) in the frequency range of 5 Hz to 13 MHz and in the temperature range of $T = 50{-}700$ °C with a heating and cooling rate of 20 K/h. The data were recorded and evaluated using the program SIGMA.[29] The dc conductivity was determined simultaneously.

All NMR experiments were performed using a Bruker DSX-400 spectrometer operating at 9.4 T with resonance frequencies of 58.9 and 155.5 MHz for ^{6}Li and ^{7}Li, respectively. Chemical shifts are referenced relative to the peak for 1 M aqueous LiCl. The samples were sealed in Pyrex tubes fitting exactly into the MAS rotor. ^{6}Li MAS, ^{7}Li MAS, and static ^{7}Li NMR experiments were recorded in the temperature range 184 K < T < 573 K employing a 7 mm Bruker WVT MAS probe.

Results and Discussion

Crystal Structures of Li$_7$MO$_6$ (M = Nb, Ta, Sb, Bi). Whereas for Li$_7$BiO$_6$ the hexagonal metric is retained at room temperature (space group $R\bar{3}$), thus confirming the published data,[7] for Li$_7$MO$_6$ (M = Nb, Ta, Sb) a triclinic metric (space

---

(28) Köhler, U. Ph.D. Thesis, University of Hannover, Germany, 1987.
(29) Henseler, U. Ph.D. Thesis, University of Bonn, Germany, 1998.

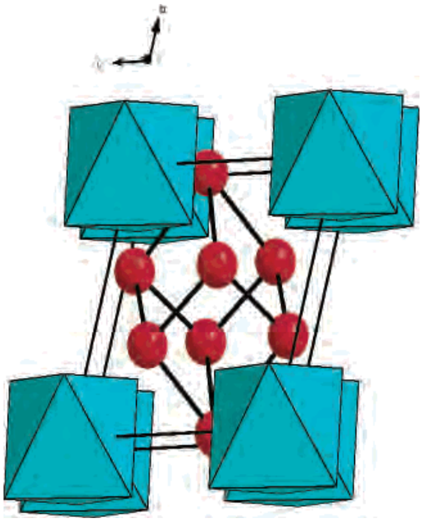

Figure 3. Crystal structure of Li_7MO_6 (M = Nb, Ta, Sb) in a projection along the *a* axis. The regular MO_6 octahedra and the lithium metal positions on the corners of a distorted cube (lithium sublattice) are drawn.

group $P\bar{1}$) is found in contrast to the single-crystal analysis by Hoppe and Wehrum.[8] This may be due to the lower resolution of the single-crystal analysis in ref 8. The lattice parameters for Li_7MO_6 (M = Nb, Ta, Sb) are given in Table 1. The number of formula units per unit cell is determined to be $Z = 1$ from packing considerations and density measurements. Niobium, tantalum, and antimony atoms are located in the origin of the triclinic unit cells and are surrounded by six oxygen atoms, forming a regular octahedron (Figure 3). Li1, Li2, and Li3 are surrounded by four oxygen atoms, forming distorted tetrahedra, whereas Li4 is surrounded by six oxygen atoms, forming a distorted octahedron. Difference Fourier analysis suggests that the eight Li positions in the unit cell are equally occupied by the seven lithium atoms, with the lithium atoms forming a distorted cube within the unit cell with a mean Li−Li distance of 2.41(14) Å (for Li_7TaO_6). The crystal structure of Li_7MO_6 (M = Nb, Ta, Sb, Bi) can be described as a slightly distorted hexagonal close packing (hcp) of oxygen atoms with 50% of the tetrahedral voids filled by lithium atoms and 50% of the octahedral voids filled by lithium and heavy metal atoms in a (ideal) ratio of 2:3. This leads to the general formula of $(M_1Li_{1.75\square 3})^{VI}(Li_{5.25\square 6})^{IV}O_6$. An alternative description of the structure would emphasize the crystal chemical relationship to the binary layered halides: neglecting the deficiencies at the Li sites, slabs of composition $M_{1/3}Li_{2/3}O_2$ are stacked as the corresponding CdI_2 layers in cadmium iodide. The remaining lithium atoms occupy half of the tetrahedral sites within the resulting gap.

The plausibility of the structure was checked by a calculation of the bond length/bond strength relations and the lattice energies using the program MAPLE.[30] The Madelung parts of the lattice energy correspond well with the sums calculated for the binary constituents. The calculated bond valence sums for the lithium atoms in Li_7SbO_6 (Li1, 1.04; Li2, 1.03; Li3, 1.10; Li4, 0.78) are close to the expected value of 1.0 except for Li4, which shows a slightly larger variation. The bond valence sums for the oxygen atoms (O1, 2.04; O2, 2.17; O3, 2.32) and for the antimony atom (5.17) agree well with the expected value. All geometrical values for the three compounds are listed in Table 4. The Coulomb part of the lattice energy of Li_7SbO_6 (7375.9 kcal/mol) almost perfectly matches the sum of the lattice energies of the reactants Li_2O and Sb_2O_3 (7399.5 kcal/mol), further validating the determined crystal structure.

Table 4. MAPLE[30] Results for Li_7SbO_6 (kcal/mol)

		Li_7SbO_6	Σ of binary compounds	δ
Sb	1×	2816.2	3005.1[a]	−188.9
O1	2×	582.8	587.5[b]	−9.4
O2	2×	567.3	0.5 × 587.5[b] 1.5 × 543.5[c]	25.6
O3	2×	570.3	543.5[c]	53.6
Li1	2×	167.1	146.2[c]	41.8
Li2	2×	153.6	146.2[c]	14.8
Li3	2×	157.4	146.2[c]	22.4
Li4	1×	162.7	146.2[c]	16.5
		7375.9	7399.5	−23.6 = 0.3%

[a] From Sb_2O_5. [b] From Sb_2O_5 (averaged). [c] From Li_2O (averaged) [d] MAPLE(Li_7SbO_6) − MAPLE(Li_2O) − MAPLE(Sb_2O_5).

Table 5. Observed Absorption Bands (cm^{-1}) in the IR and Raman Spectra for Compounds Li_7MO_6 (M = Ta, Nb, Sb, Bi) and Li_8MO_6 (M = Sn, Pb, Zr, Hf)[a]

	IR	Raman	ν_s(MO) (Raman)
Li_7TaO_6	390, 560	241, 450, 536, 634, 759	759
Li_7NbO_6	407, 542	187, 240, 318, 368, 444, 706, 761, 790	790 (790)[12]
Li_7SbO_6	470, 620	214, 352, 441, 534, 684	684
Li_7BiO_6	352, 428, 555	196, 424, 459, 511, 618	618 (590)[12]
Li_8SnO_6	244, 278, 306, 353, 388, 469, 568, 568, 615	204, 279, 361, 411, 450, 467, 524, 587, 636	636 (640)[12]
Li_8PbO_6	249, 275, 362, 435, 531, 583	190, 266, 377, 383, 420, 509, 572, 603	603 (600)[12]
Li_8ZrO_6	243, 295, 376, 450, 570, 640	202, 273, 414, 462, 526, 618, 668	668
Li_8HfO_6	219, 299, 369, 455, 560, 630	206, 279, 423, 475, 531, 625, 677	677 (530)[12]

[a] The ν_s(MO) (Raman) of the literature are given in parentheses.

Spectroscopy. The observed bands of the IR and Raman spectra with the ν_s(MO) vibration (from Raman) are given in Table 5. Concerning the significant reduction of symmetry as compared to Li_8MO_6, one might expect more complex vibrational spectra of Li_7MO_6 with more split absorption bands. However, the MO and LiO valence vibrations cannot be correlated to the broad bands at 200−600 cm^{-1} due to a very strong absorption of the Li_7MO_6 compounds as described.[12]

Like the IR spectra, also the Raman spectra of Li_8MO_6 provide more information than those of Li_7MO_6. This can be explained by a higher dynamic motion of the lithium cations in the lithium-deficient compounds, which is responsible for the strong absorption (see the results of ^6Li and ^7Li NMR below). The strongest band in all Raman spectra can be assigned to the hexaoxometalate octahedron. The observed ν_s(MO) bands of Li_7NbO_6, Li_7BiO_6, Li_8SnO_6, and Li_8PbO_6 are in good agreement with the results reported previously,[12] whereas Li_8HfO_6 is quite different. The Raman spectra of

---

(30) Hübenthal, R. MAPLE 4.0. Ph.D. Thesis, University of Giessen, Germany, 1991.

Table 6. Temperatures (°C) of Phase Transitions for Li_7MO_6 (M= Ta, Sb, Bi)

	X-ray powder diffraction data		DSC (onsets of peaks)		
Li_7TaO_6	200[a]	270[b]	223[a]	294[b]	379 + 387[c]
Li_7SbO_6	135[a]		167[a]		398 + 453[c]
Li_7BiO_6		150[b]		180[b]	403[c]

[a] Phase transition triclinic−rhombohedral. [b] Anisotropic expansion. [c] Melting of the lithium sublattice.

the Zr and Hf compounds are very similar and present a double band instead of the strong single band. We expect that the ν_s(MO) vibration of Li_8ZrO_6 and Li_8HfO_6 might be at 670 cm^{-1}.

High-Temperature X-ray Powder Diffractometry and DSC. Table 6 contains a compilation of data for the phase transitions in Li_7MO_6 (M = Ta, Sb, Bi) as determined by temperature-dependent Guinier recording and DSC. The temperature-dependent X-ray powder diffraction patterns of both triclinic compounds Li_7SbO_6 and Li_7TaO_6 reveal a phase transition to rhombohedral symmetry at $T = 135$ °C (for Li_7SbO_6) and $T = 200$ °C (for Li_7TaO_6). These phase transitions are also detected in the DSC measurements with a shift of approximately 30 K due to the fast heating rate of 10 K/min. In Li_7BiO_6, the rhombohedral symmetry is maintained to ambient temperature. Anisotropic thermal expansion can be noticed at some reflections in the high-temperature X-ray powder patterns at $T = 150$ °C (for Li_7BiO_6) and at $T = 270$ °C (for Li_7TaO_6) and also by a small endothermic peak in the DSC measurements. In the DSC measurements of Li_7TaO_6 and Li_7SbO_6, two strong endothermic peaks at higher temperature (380−450 °C) can be observed, which might be explained by the melting of the lithium sublattice. This is corroborated by a drastic increase in ionic conductivity around 400 °C, as evidenced by the impedance data.

Ionic Conductivity. The Arrhenius plots of the temperature-dependent ionic conductivity for Li_7MO_6 (M = Ta, Sb, Bi) are collected in Figure 4. For comparison, the data for some standard fast lithium ion conductors are included in this figure. In Table 7, the corresponding activation energies (E_a) as derived from the slopes of the conductivity curves using the Arrhenius equation are compiled.

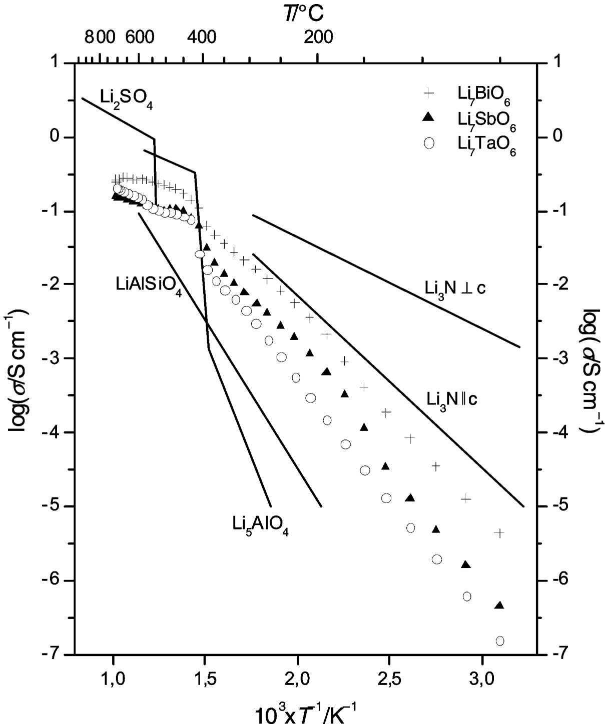

Figure 4. Ionic conductivity heating plots of Li_7MO_6 (M = Ta, Sb, Bi) in comparison with well-known fast lithium conductors.[31]

Table 7. Ionic Conductivities (σ) and the Activation Energies (E_a) of the Heating Plot for Li_7MO_6 (M = Ta, Sb, Bi)[a]

	σ (S cm^{-1})	E_a (eV)
Li_7TaO_6	50 °C: 1.53×10^{-7} (0.84×10^{-7})[15]	50-400 °C: 0.68 (0.67)[15]
	300 °C: 3.76×10^{-3} (1.05×10^{-3})[15]	400−700 °C: 0.29
	700 °C: 0.2028	
Li_7SbO_6	50 °C: 4.58×10^{-7}	50−170 °C: 0.70
	300 °C: 6.58×10^{-3}	170−400 °C: 0.53
	700 °C: 0.1531	400−700 °C: 0.20
Li_7BiO_6	50 °C: 43.48×10^{-7} (6.84×10^{-7})[15]	50−200 °C: 0.58 (0.68)[15]
	300 °C: 18.64×10^{-3} (7.89×10^{-3})[15]	200−400 °C: 0.48
	700 °C: 0.2631	400−700°C: 0.27

[a] Literature values are given in parentheses.

As mentioned above, the conductivity curves of all three Li_7MO_6 compounds show a drastic change in the slopes at approximately $T = 400$ °C. In addition, for Li_7SbO_6 a slight change in the slope of the conductivity curve at $T = 170$ °C can be observed, in good agreement with the phase transition from triclinic to rhombohedral symmetry as revealed by temperature-dependent Guinier recording and DSC. Li_7BiO_6 also exhibits a slight change in the slope of the conductivity curve at $T = 200$ °C which might be due to the anisotropic thermal expansion detected by the temperature-dependent Guinier recording and DSC. This effect was not observed in the conductivity curves of the other two compounds. In comparison to the results of Nomura and Greenblatt,[15] the ionic conductivities and activation energies of Li_7TaO_6 match quite well, whereas in the case of Li_7BiO_6 we measured higher ionic conductivities and lower activation energies, which can possibly be explained by a different preparation of the samples used for the conductivity measurements. All three substances as described here exhibit a high ionic conductivity over a wide temperature range in comparison with other known fast ionic conductors (cf. Figure 4).[31]

NMR Spectroscopy. The ^6Li and ^7Li NMR experiments were performed to further elucidate the nature of lithium mobility in the studied hexaoxometalates. NMR has been shown to be a very valuable tool in the characterization of dynamic processes in solids. Processes with correlation times in the range of 10^{-2} to 10^{-5} s can be studied via their influence on the NMR line shape. If the reciprocal correlation time approaches the width of the NMR line, determined by the anisotropic spin interactions, then the fluctuations in the spin interactions entail a motional narrowing of the NMR

---

(31) Kudo, T.; Fueki, K. *Solid State Ionics*; VCH−Verlag: Weinheim, Germany, 1990; p 123.

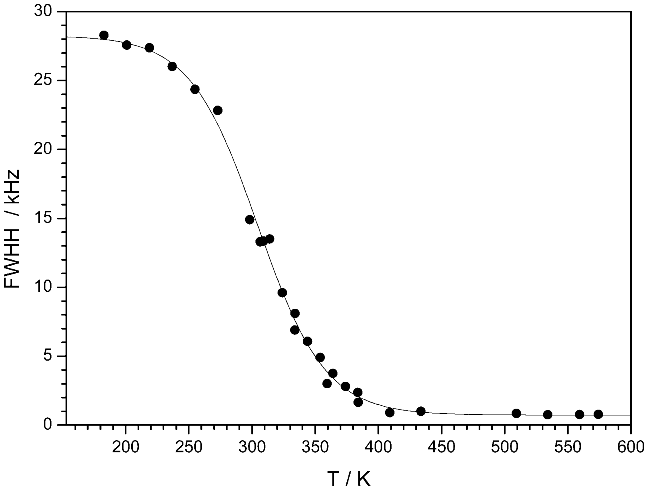

Figure 5. ^{7}Li NMR line width (full width at half-height, fwhh) of the central transition as a function of temperature for Li_7TaO_6.

line.[32,33] In Figure 5, the width of the central ($m = -{}^1/_2 \rightarrow m = +{}^1/_2$) ^{7}Li NMR line is plotted as a function of temperature. Starting with a line width of approximately 17 kHz at room temperature, the width of the ^{7}Li NMR line is gradually reduced until at $T = 150$ °C a constant value of approximately 1 kHz is reached. These results clearly demonstrate that the lithium ions are mobile even at temperatures as low as 50 °C. The value of 1 kHz for the ^{7}Li NMR line width at temperatures above 130 °C indicates rapid lithium motion in this phase. Note that neither in the DSC nor in the high-temperature diffraction did we find any reference to this motion. This possibly indicates a local exchange of lithium cations among the octahedral and tetrahedral positions. To address this question further, we performed temperature-dependent ^{6}Li MAS NMR experiments. Although the chemical shift range of the Li isotopes covers only a few parts per million on the chemical shift scale, a distinction between different Li sites is possible using the ^{6}Li isotope. For ^{6}Li (natural abundance 7.4%) the quadrupolar moment (-8.1×10^{-32} m^{-2}) is approximately 50 times smaller than that for ^{7}Li. Thus, the ^{6}Li MAS NMR signal is not expected to be affected by quadrupolar or homonuclear dipolar interaction, resulting in a distinctively enhanced spectral resolution as compared to the corresponding ^{7}Li MAS NMR signal. This is corroborated by the results presented in Figure 6. In Figure 6a the room-temperature spectra of the ^{6}Li MAS and ^{7}Li MAS NMR lines are compared; Figure 6b contains a collection of ^{6}Li MAS NMR spectra in the temperature range $184 < T < 475$ K. The increased resolution of the ^{6}Li MAS line shape compared to the ^{7}Li MAS line (broadened by strong homonuclear dipolar and quadrupolar interaction) is obvious from inspection of Figure 6; three individual signals at −0.3, 1.1, and 1.9 ppm can be identified. Using the Li chemical shift ↔ Li coordination number correlation established by Stebbins using a series of lithium aluminosilicates and lithium silicates[34] as a

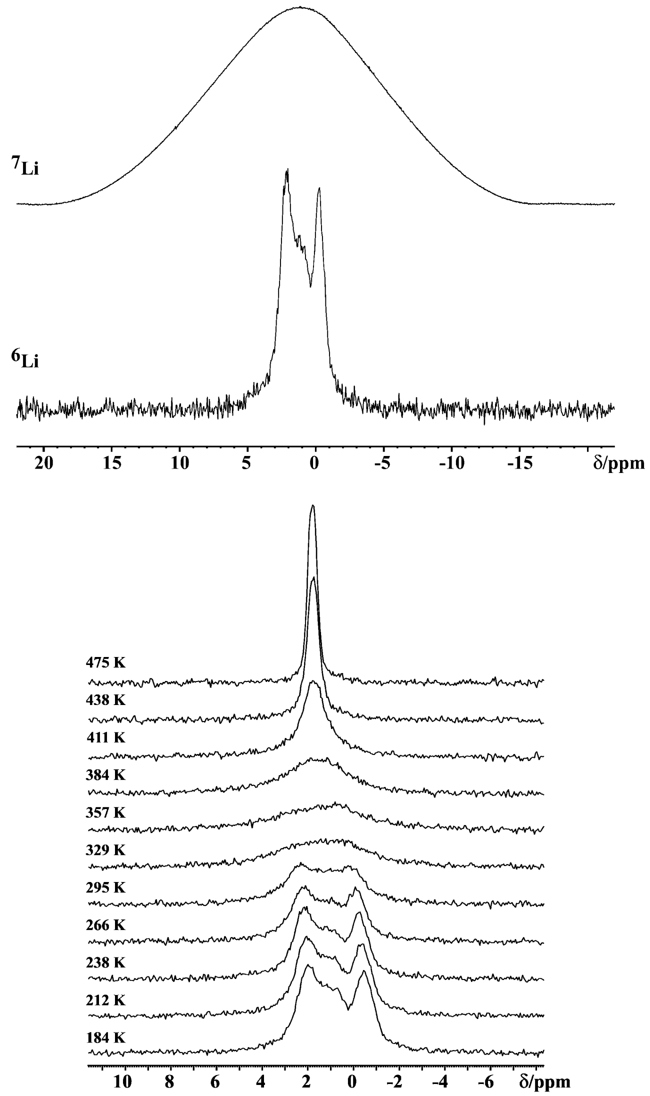

Figure 6. (a, top) ^{7}Li MAS NMR and ^{6}Li MAS NMR spectra of Li_7TaO_6 at 238 K illustrating the superior resolution of the ^{6}Li MAS NMR line shape. (b, bottom) ^{6}Li MAS NMR spectra as a function of temperature for Li_7TaO_6.

basis for our discussion, we tentatively assign the signal at −0.3 ppm as arising from the lithium atoms, octahedrally coordinated by oxygen (Li4) and the signals at 1.1 and 1.9 ppm to lithium atoms in tetrahedral voids. Although a deconvolution into individual resonances proves too difficult due to considerable peak overlap, from inspection of Figure 6b it is clear that the three signals merge into a single resonance at temperatures above 333 K. This is a signature of lithium cations exchanging between octahedral and tetrahedral sites on a time scale fast compared to the corresponding NMR time scale, i.e., 10^2 to 10^3 Hz.

Conclusion

The structures, phase transitions, and ionic conductivities of the lithium hexaoxometalates Li_8MO_6 (M = Sn, Pb, Zr, Hf) and Li_7MO_6 (M = Nb, Ta, Sb, Bi) have been studied using powder X-ray synchrotron diffraction tech-

---

(32) Abragam, A. *The Principles of Nuclear Magnetism*; Clarendon Press: Oxford, 1961.

(33) Slichter, C. P. *Principles of Nuclear Magnetic Resonance*; Springer: Berlin, 1996.

(34) Xu, Z.; Stebbins, J. F. *Solid State Nucl. Magn. Reson.* **1995**, *5*, 103−112.

niques, high-temperature Guinier and DSC, impedance spectroscopy, and solid-state NMR. The triclinic structures of Li_7MO_6 (M = Ta, Nb, Sb) deviate from the rhombohedral lattice typical for all remaining known alkali-metal hexaoxometalates. The solid-state NMR data are consistent with the assumption of mobile Li ions even at ambient temperatures, performing local jumps between tetrahedral and octahedral voids. The observed phase transitions at elevated temperatures ($T \approx 400$ °C), accompanied by an increase in the ionic conductivity, indicate a major change in the structural arrangement. Since no response to these phase transitions is found in the temperature-dependent X-ray diffraction patterns, it is assumed that the phase transitions are accompanied by a melting of the lithium cation sublattice.

Further work including high-temperature solid-state NMR experiments is currently being performed in our laboratory to further elucidate the nature of the high-temperature phase transitions.

Acknowledgment. We thank Dr. Helmut Haas for structural work in the early stages of the project. Research was carried out in part at the National Synchrotron Light Source (NSLS). Financial support by the Fonds der Chemischen Industrie (FCI) and the Bundesministerium für Bildung und Forschung (BMBF) is gratefully acknowledged.

Supporting Information Available: Table listing the crystallographic data for Li_7MO_6 (M = Nb, Sb, Ta). This material is available free of charge via the Internet at http://pubs.acs.org.

IC030208W